

## Design of Injection and Recombination in Quantum Dot Sensitized Solar Cells

Eva M. Barea,<sup>†</sup> Menny Shalom,<sup>‡</sup> Sixto Giménez,<sup>†</sup> Idan Hod,<sup>‡</sup> Iván Mora-Seró,<sup>\*,†</sup> Arie Zaban,<sup>‡</sup> and Juan Bisquert<sup>†</sup>

*Photovoltaic and Optoelectronic Devices Group, Departament de Física, Universitat Jaume I, 12071 Castelló, Spain and Institute of Nanotechnology & Advanced Materials, Department of Chemistry, Bar Ilan University, 52900 Ramat Gan, Israel*

Received March 2, 2010; E-mail: sero@fca.uji.es

**Abstract:** Semiconductor Quantum Dots (QDs) currently receive widespread attention for the development of photovoltaic devices due to the possibility of tailoring their optoelectronic properties by the control of size and composition. Here we show that it is possible to design both injection and recombination in QD sensitized solar cells (QDSCs) by the appropriate use of molecular dipoles and conformal coatings. QDSCs have been manufactured using mesoporous TiO<sub>2</sub> electrodes coated with “in situ” grown CdSe semiconductor nanocrystals by chemical bath deposition (CBD). Surface modification of the CdSe sensitized electrodes by conformal ZnS coating and grafting of molecular dipoles (DT) has been explored to both increase the injection from QDs into the TiO<sub>2</sub> matrix and reduce the recombination of the QD sensitized electrodes. Different sequences of both treatments have been tested aiming at boosting the energy conversion efficiency of the devices. The obtained results showed that the most favorable sequence of the surface treatment (DT+ZnS) led to a dramatic 600% increase of photovoltaic performance compared to the reference electrode (without modification):  $V_{oc} = 0.488$  V,  $j_{sc} = 9.74$  mA/cm<sup>2</sup>, FF = 0.34, and efficiency = 1.60% under full 1 sun illumination. The measured photovoltaic performance was correlated to the relative position of the CdSe conduction band (characterized by surface photovoltage measurements) and TiO<sub>2</sub> conduction band (characterized by the chemical capacitance,  $C_{\mu}$ ) together with recombination resistance,  $R_{rec}$ .

### 1. Introduction

Quantum dot sensitized solar cells (QDSCs) constitute one of the most promising low cost candidates for third generation photovoltaics.<sup>1–4</sup> This solar cell concept is borrowed from the photoelectrochemical Gratzel’s cell, the dye sensitized solar cell (DSC),<sup>5</sup> which is based on a mesoporous structure of a wide band semiconductor material (e.g., TiO<sub>2</sub>, ZnO...) sensitized by a light harvesting material (conventionally metallorganic Ru-based dyes), permeated with a redox electrolyte, and sandwiched by a counterelectrode. The formal difference between QDSCs and DSCs relies on the use of semiconductor nanocrystals (QDs) instead of dyes as light absorber materials. QDs exhibit several advantages with respect to metallorganic dyes as light absorbers related to tunable band gaps by size control,<sup>6</sup> higher molar extinction coefficients,<sup>7</sup> and large intrinsic dipole moments<sup>8,9</sup> enhancing charge separation. However, at present, the record

solar conversion efficiencies of QDSCs (3–4%)<sup>10,11</sup> lag behind DSCs (11.4%)<sup>12</sup> by a factor of 3–4, although progressive optimization of the former is expected to narrow the actual gap.

The replacement of the light harvesting material in the solar cell configuration requires a full modification process involving a general substitution of the other components to preserve the favorable band alignment for charge separation, charge transfer processes, and QD stability.<sup>13,14</sup> Additionally, the competition between injection, transport, and recombination kinetics must remain favorable for efficient conversion efficiency together with chemical compatibility of the full device. As an example, the standard I<sup>-</sup>/I<sub>3</sub><sup>-</sup> redox couple employed for DSCs is not chemically compatible with QDs leading to fast degradation of the nanocrystals. Consequently, nanometric barriers between QDs and electrolyte must be included<sup>15,16</sup> to maintain chemical compatibility, or alternatively, different redox systems must be

<sup>†</sup> Universitat Jaume I.

<sup>‡</sup> Bar Ilan University.

- (1) Nozik, A. J. *Physica E* **2002**, *14*, 115.
- (2) Klimov, V. I. *J. Phys. Chem. B* **2006**, *110*, 16827.
- (3) Kamat, P. V. *J. Phys. Chem. C* **2008**, *112*, 18737.
- (4) Hodes, G. J. *Phys. Chem. C* **2008**, *112*, 17778.
- (5) O’Regan, B.; Gratzel, M. *Nature* **1991**, *353*, 737.
- (6) Yu, W.; Qu, L. H.; Guo, W. Z.; Peng, X. G. *Chem. Mater.* **2003**, *15*, 2854.
- (7) Wang, P.; Zakeeruddin, S. M.; Moser, J. E.; Humphry-Baker, R.; Comte, P.; Aranyos, V.; Hagfeldt, A.; Nazeeruddin, M. K.; Gratzel, M. *Adv. Mater.* **2004**, *16*, 1806.
- (8) Vogel, R.; Hoyer, P.; Weller, H. *J. Phys. Chem. B* **1994**, *98*, 3183.
- (9) Vogel, R.; Pohl, K.; Weller, H. *Chem. Phys. Lett.* **1990**, *174*, 241.

- (10) Diguna, L. J.; Shen, Q.; Kobayashi, J.; Toyoda, T. *Appl. Phys. Lett.* **2007**, *91*, 0231161.
- (11) Fan, S.-Q.; Fang, B.; Kim, J. H.; Kim, J.-J.; Yu, J.-S.; Ko, J. *Appl. Phys. Lett.* **2010**, *96*, 063501.
- (12) Cao, Y.; Bai, Y.; Yu, Q.; Cheng, Y.; Liu, S.; Shi, D.; Gao, F.; Wang, P. *J. Phys. Chem. C* **2009**, *113*, 6290.
- (13) Mora-Seró, I.; Giménez, S.; Fabregat-Santiago, F.; Gómez, R.; Shen, Q.; Toyoda, T.; Bisquert, J. *Acc. Chem. Res.* **2009**, *42*, 1848.
- (14) Lee, H. J.; Yum, J.-H.; Leventis, H. C.; Zakeeruddin, S. M.; Haque, S. A.; Chen, P.; Seok, S. I.; Grätzel, M.; Nazeeruddin, M. K. *J. Phys. Chem. C* **2008**, *112*, 11600.
- (15) Shalom, M.; Dor, S.; Rühle, S.; Grinis, L.; Zaban, A. *J. Phys. Chem. C* **2009**, *113*, 3895.
- (16) Shalom, M.; Albero, J.; Tachan, Z.; Martínez-Ferrero, E.; Zaban, A.; Palomares, E. *J. Phys. Chem. Lett.* **2010**, *1*, 1134.

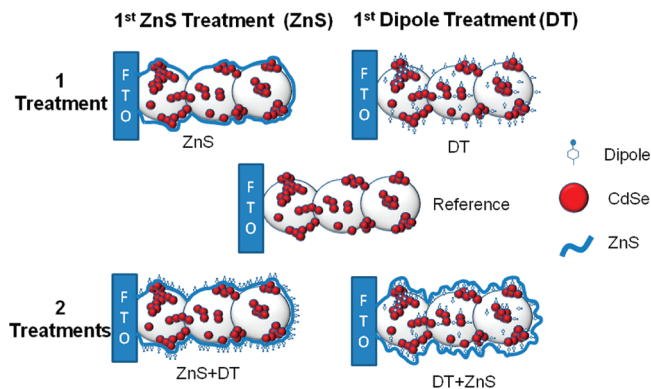


**Figure 1.** Different sensitized electrode configurations analyzed in this study. Sample after CBD growth with no treatment is taken as reference sample. Two configurations with only one treatment have been analyzed: with ZnS coating (ZnS sample) and with dipole grafting (DT sample). In addition, samples with two treatments: first DT and second ZnS coating (DT+ZnS) and first ZnS coating and second a dipole treatment (ZnS+DT) have been explored.

incorporated as the polysulfide<sup>17–19</sup> or Co-based<sup>14,20</sup> systems. Moreover, the electrocatalytic activity of the Pt counterelectrodes conventionally used for DSCs is poor<sup>17,21,22</sup> and thus unable to regenerate the polysulfide electrolyte leading to high series resistances, and more suitable materials should be employed (Au, Cu<sub>2</sub>S, CoS, etc.).<sup>11,17,22,23</sup>

On the other hand, surface modification via different approaches has demonstrated to be a powerful tool to boost the energy conversion efficiencies of the devices. For example, tailoring the band alignment of wide band semiconductors as TiO<sub>2</sub> and CdS semiconductor nanocrystals through surface modification with molecular dipoles<sup>24</sup> leads to a significant increase in energy conversion efficiency in QDSCs. Additionally, coating the TiO<sub>2</sub>/CdSe nanoporous structure with ZnS nanometric barriers<sup>23,25</sup> results in almost doubling the efficiency of these solar cells mainly due to a significant increase of the recombination resistance between TiO<sub>2</sub> and the electrolyte.<sup>13</sup>

In the present study, the main objective is exploring the beneficial effects of both surface treatments leading to the increased performance of the devices. Therefore, different sequences of both treatments, see Figure 1, have been tested searching for the optimum synergistic interaction between them tailoring both charge injection and recombination dynamics, observing a dramatic effect in cell performance related with the treatments applied.

## 2. Experimental Section

**Electrode Configuration.** The mesoporous TiO<sub>2</sub> working electrodes used for the present study were processed by two different approaches. Some films were prepared by electrophoretic deposition (EPD) of Degussa P25 Particles onto SnO<sub>2</sub>:F (FTO).<sup>26</sup> The electrodes were deposited through two consecutive cycles of 30 s at a constant current density of 0.4 mA/cm<sup>2</sup> with an intermediate drying step at 120 °C for ~5 min. Following the EPD process, these electrodes were dried in air at 150 °C for 30 min, pressed at 800 kg/cm<sup>2</sup> using a hydraulic press, and sintered at 550 °C for 1 h. The average thickness of the EPD electrodes was 5 μm.

Some other electrodes were manufactured by doctor blading using commercial TiO<sub>2</sub> pastes provided by Dyesol (Queansbeyan, Australia). The electrode configuration was a transparent layer DSL 18NR-T (20 nm average particle size) and a scatter layer 18NR-AO (20–450 nm particle size distribution). The FTO coated glass was previously covered by a compact layer of TiO<sub>2</sub> deposited by spray pyrolysis of titanium(IV)bis(acetoacetonato) di(isopropanoxy)late. These electrodes were sintered at 450 °C for 30 min. The thickness of the mesoporous electrodes was ~10 μm measured by a Dektack 6 profilometer from Veeco.

The mesoporous TiO<sub>2</sub> electrodes were “in situ” sensitized by CdSe QDs grown by chemical bath deposition (CBD) following the procedure published by Gorer and Hodes.<sup>27</sup> First, as the Se source, an 80 mM sodium selenosulphate (Na<sub>2</sub>SeSO<sub>3</sub>) solution was prepared by dissolving elemental Se powder in a 200 mM Na<sub>2</sub>SO<sub>3</sub> solution. Second, 80 mM CdSO<sub>4</sub> and 120 mM trisodium salt of nitrilotriacetic acid (N(CH<sub>2</sub>COONa)<sub>3</sub>) were mixed at a volume ratio of 1:1. Finally, both solutions were mixed at a volume ratio of 1:2. The mesoporous TiO<sub>2</sub> electrodes were placed in a glass container filled with the final solution for a 30 h deposition time at 10 °C under darkness.

The as-sensitized electrodes were subsequently modified by applying different surface treatments. Dipole treatment (DT): the electrode is immersed in a 10 mM ethanol solution of different benzenethiol (BT) derivatives overnight<sup>24</sup> (4-methoxybenzenethiol (BTOCH<sub>3</sub>), 4-methylbenzenethiol (BTCH<sub>3</sub>), 4-fluorobenzenethiol (BTF), 4-nitrobenzenethiol (BTNO<sub>2</sub>)); see inset Figure 2a. For the ZnS treatment, the electrodes were coated with ZnS by twice dipping alternately into 0.1 M Zn(CH<sub>3</sub>COO)<sub>2</sub> and 0.1 M Na<sub>2</sub>S solutions for 1 min/dip, rinsing with Milli-Q ultrapure water between dips.<sup>25</sup>

**Solar Cell Configuration.** The solar cells were prepared by assembling a Pt counter electrode and a QD sensitized FTO/TiO<sub>2</sub> electrode (with the corresponding surface treatment). The solar cells prepared with doctor-bladed electrodes were sealed using a Surlyn (Dupont) thermoplastic frame (25 μm thick). Conversely, a PTFE spacer (40 μm thick) was used to frame the cells mounted with EPD electrodes. A standard redox polysulfide electrolyte was used in all cases. It was prepared following the procedure described in ref 28: 1 M Na<sub>2</sub>S, 1 M S, and 0.1 M NaOH solution in Milli-Q ultrapure water.

**Optical and Electrical Characterization.** Photovoltage spectroscopy (PVS) is a sensitive tool to detect the onset of electron injection from an absorber into the electron conductor such as TiO<sub>2</sub>. The signal onset is defined as the energy at which the PVS signal has reached 20% of its maximum value. Photocurrent–voltage characteristics were performed with an Eco-Chemie Potentiostat. A 250 W xenon arc lamp (Oriol) served as a light source for PVS and incident photon to current efficiency (IPCE).

The diffuse reflectance spectra were recorded by a Cary 5000 UV–vis–NIR Varian spectrophotometer equipped with an integration sphere. The optical density (OD) was displayed as  $F(R) =$

(17) Hodes, G.; Manassen, J.; Cahen, D. *Electrochem. Soc.* **1980**, *127*, 544.

(18) Lee, Y.-L.; Chang, C.-H. *J. Power Sources* **2008**, *185*, 584.

(19) Robel, I.; Subramanian, V.; Kuno, M.; Kamat, P. V. *J. Am. Chem. Soc.* **2006**, *128*, 2385.

(20) Lee, H. J.; Wang, M.; Chen, P.; Gamelin, D. R.; Zakeeruddin, S. M.; Grätzel, M.; Nazeeruddin, M. K. *Nano Lett.* **2009**, *9*, 4221.

(21) Licht, S.; Khaselev, O.; Ramakrishnan, P. A.; Soga, T.; Umeno, M. *J. Phys. Chem. B* **1998**, *102*, 2536.

(22) Mora-Seró, I.; Giménez, S.; Moehl, T.; Fabregat-Santiago, F.; Lana-Villareal, T.; Gómez, R.; Bisquert, J. *Nanotechnology* **2008**, *19*, 4240071.

(23) Giménez, S.; Mora-Seró, I.; Macor, L.; Guijarro, N.; Lana-Villareal, T.; Gómez, R.; Diguna, L. J.; Shen, Q.; Toyoda, T.; Bisquert, J. *Nanotechnology* **2009**, *20*, 295204.

(24) Shalom, M.; Rühle, S.; Hod, I.; Yahav, S.; Zaban, A. *J. Am. Chem. Soc.* **2009**, *131*, 9876.

(25) Shen, Q.; Kobayashi, J.; Diguna, L. J.; Toyoda, T. *J. Appl. Phys.* **2008**, *103*, 084304.

(26) Grinis, L.; Dor, S.; Ofir, A.; Zaban, A. *J. Photochem. Photobiol., A* **2008**, *198*, 52.

(27) Gorer, S.; Hodes, G. *J. Phys. Chem.* **1994**, *98*, 5338.

(28) Zhao, P.; Zhang, H.; Zhou, H.; Yi, B. *Electrochim. Acta* **2005**, *51*, 1091.

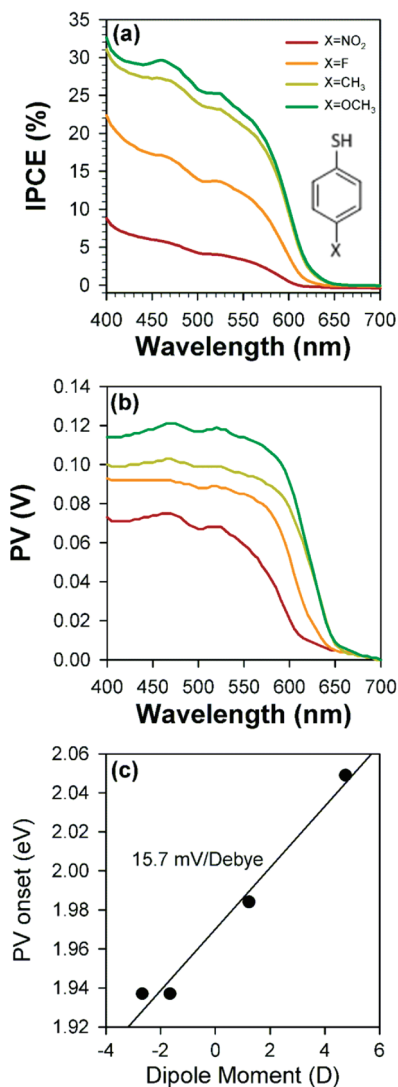


**Figure 2.** (a) Incident photon to current efficiency (IPCE) measurements of CdSe QD sensitized EPD TiO<sub>2</sub> electrodes, modified with a series of BT derivatives, show a dipole dependent photoresponse; the inset shows the benzenethiol (BT) molecular structure. (b) PV spectroscopy of the same samples. (c) PV onset as function of the molecular dipole moment (symbols), and linear regression fit (solid line).

$(1 - R)^2/2R$  in Kubelka–Munk units, where  $R$  is the measured diffuse reflectance. Current–potential curves and impedance spectroscopy measurements were obtained using an FRA equipped PGSTAT-30 from Autolab. The cells were illuminated using a solar simulator at AM 1.5 G, where the light intensity was adjusted with an NREL-calibrated Si solar cell with a KG-5 filter to a 1 sun intensity ( $100 \text{ mW cm}^{-2}$ ). Impedance spectroscopy (IS) measurements were carried out in dark conditions at forward bias: 0–0.5 V, applying a 20 mV AC sinusoidal signal over the constant applied bias with the frequency ranging between 500 kHz and 0.1 Hz.

### 3. Results and Discussion

Mesoporous TiO<sub>2</sub> sensitized with CdSe QDs prepared by CBD exhibit a dramatic change in the photovoltaic conversion efficiency, after modification with benzenethiol (BT) derivatives; see Figure 2a. This figure illustrates the incident photon-to-current efficiency (IPCE) for QD sensitized electrodes with different BT molecular dipoles grafted onto the TiO<sub>2</sub>/CdSe mesoporous structure. Depending on the maximum IPCE values measured, the different BT derivatives employed can be ranked

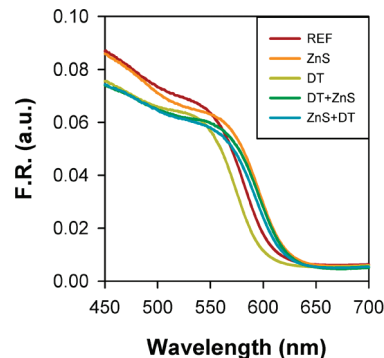


**Figure 3.** Diffuse reflectivity spectra of mesoporous doctor-bladed TiO<sub>2</sub> substrates sensitized with CdSe QDs after different surface treatments.

as  $\text{BTOCH}_3 > \text{BTCH}_3 > \text{BTF} > \text{BTNO}_2$ , oppositely following the trend of the molecular dipole moments  $-2.67 < -1.66 < 1.23 < 4.76 \text{ D}^{24}$  respectively. As previously reported for CdS QDSCs, more negative dipole moments are correlated to higher values of IPCE as a consequence of the upward shift of the conduction band (CB) of QDs.

CBD grown QDs exhibit a broad size dispersion. Larger QDs with a narrower band gap show a lower electron transfer rate constant due to the progressive decrease of the band offset between CdSe and TiO<sub>2</sub>, leading to less favorable energetic conditions for charge injection.<sup>29</sup> The upward shift of the CB of CdSe QDs allows larger QDs with a low or null electron transfer rate to increase their electron injection rate into TiO<sub>2</sub>. This effect can be better observed by photovoltage spectroscopy (PVS), more sensitive than IPCE at lower injection rates; see Figure 2b. In this figure, a systematic shift of the photovoltage onset to higher wavelength values is observed as the dipole moment of the molecule used moves toward more negative values. Taking into account the photovoltage onset for each molecular dipole, the apparent shift of the CB of CdSe QDs can be quantified as 15.7 meV/D (Figure 2c). This value is lower compared to that calculated for CdS QDs (21.7 meV/D).<sup>24</sup> The origin of this variation is the higher dielectric constant of CdSe.

The best photovoltaic performance can be anticipated for the BTOCH<sub>3</sub> derivative, and only this molecule was selected for further investigation. As already mentioned, conformal ZnS coating of CdSe QD sensitized electrodes also improves the performance of QDSCs.<sup>13,23,25</sup> To evaluate the optimum synergistic interaction between different surface modification treatments, the grafting of molecular dipoles together with the deposition of a ZnS coating was tested; see Figure 1. Figure 3 illustrates the optical density (OD) of the nanostructured photoanodes with different sequences of surface treatments. From comparison with the reference sample (CdSe sensitized electrode without any surface treatment), slight blue shifts and a decrease in intensity of the excitonic absorption band of CdSe are observed after treatment with BTOCH<sub>3</sub>. This effect can be attributed to the capping of QDs with BTOCH<sub>3</sub> as the capping molecule has an influence on both absorption peak position and absorption intensity as has been previously reported.<sup>30</sup> The ZnS coating leads to an  $\sim 10\%$  increase in OD and a slight red shift due to the loss of quantum confinement of the electron wave function.<sup>23</sup> Additionally, in terms of OD, the combination of both treatments is practically commutative.

(29) Robel, I.; Kuno, M.; Kamat, P. V. *J. Am. Chem. Soc.* **2007**, *129*, 4136.

(30) Dorokhin, D.; Tomczak, N.; Mingyong, H.; Reinhoudt, D. N.; Velders, A. H.; Vancso, G. J. *ACS Nano* **2010**, *3*, 661.



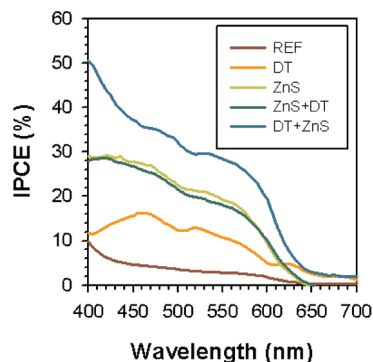


**Figure 4.** IPCE spectra of QDSCs with different surface treatments using doctor-bladed TiO<sub>2</sub> substrates.

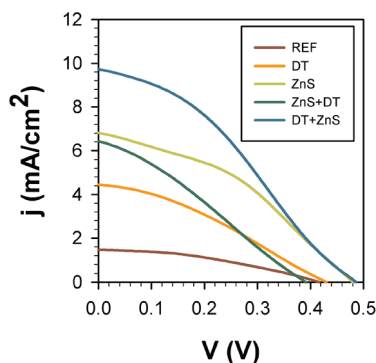


**Figure 5.**  $j$ - $V$  curves of sealed solar cells prepared with doctor-bladed mesoporous electrodes after different surface treatments.

**Table 1.** Photovoltaic Properties of the Manufactured Solar Cells As a Function of the Different Surface Modifications Tested under Standard Conditions (100 mW/cm<sup>2</sup> AM 1.5)<sup>a</sup>

Specimens	$V_{oc}$ (V)	$j_{sc}$ (mA/cm <sup>2</sup> )	FF	$\eta$ (%)	$\Delta E_{CB-TiO_2}$ (eV)
Reference	0.420	1.47	0.37	0.23	0
ZnS	0.483	6.81	0.38	1.25	0.08
DT	0.435	4.46	0.32	0.63	0.08
ZnS+DT	0.396	6.43	0.29	0.71	0.075
DT+ZnS	0.488	9.74	0.34	1.60	0.1

<sup>a</sup> The displacement of the TiO<sub>2</sub> CB observed by IS (see Figure 6) is also included.

The IPCEs of the solar cells manufactured with these photoanodes are reported in Figure 4. The reference cell shows a low IPCE below 10% for the full spectral range analyzed. After grafting of the OCH<sub>3</sub> molecular dipole, IPCE is substantially increased although, for this set of specimens, the values are lower compared to those reported in Figure 2a, corresponding to a different batch of samples. A higher enhancement in IPCE is obtained after ZnS conformal coating of the reference electrodes. On the other hand, when both treatments (ZnS and DT) are sequentially applied, the effect on the IPCE is not commutative. Indeed, the application of the DT treatment onto a ZnS coated electrode leads to a slight reduction of IPCE compared to the sample with only a ZnS coating. Conversely, the application of ZnS after the DT leads to the maximum IPCE value (~30% at 500–600 nm) for this combination of surface modifications. This trend is mimicked by the  $j$ - $V$  curves for the solar cells with the different surface modifications tested in the present study (Figure 5). Table 1 summarizes the photovoltaic properties obtained. Note that two different sets of samples were used for IPCE and  $j$ - $V$  measurements. Compared to the reference, the open circuit voltage,  $V_{oc}$ , slightly increases

for the sample after DT. A considerably higher increase of photovoltage is observed for the ZnS and DT+ZnS samples, whereas a decrease of  $V_{oc}$  is observed for the ZnS+DT specimen. The fill factors, FF, are systematically low, ranging 0.3–0.4 as expected for an alternative recombination path for electrons via surface states of TiO<sub>2</sub><sup>13</sup> and from the high charge transfer resistance between the polysulfide redox and platinized counter electrode.<sup>22,31</sup> However, the main effect of the surface treatments on the solar cell performance is reflected on the short circuit current,  $j_{sc}$ , which is proportional to the efficiency following exactly the same tendency reported for IPCE; see Figures 4 and 5. The maximum  $j_{sc}$  value obtained for the DT+ZnS sample, ~10 mA/cm<sup>2</sup>, is more than six times higher compared to the reference sample, leading to a 1.60% photovoltaic conversion efficiency under full 1 sun illumination and a 600% increase in the cell performance compared with the reference sample.

To highlight the origin of the dramatic increase of photocurrent after the different surface treatments, impedance spectroscopy has been carried out under dark conditions at varying forward applied bias. The obtained IS spectra are characterized by the presence of two semiarcs in a Nyquist plot (not shown).<sup>13</sup> The high frequency semiarc is related to the charge transfer at the counter electrode, and the low-frequency arc includes the chemical capacitance of nanostructured TiO<sub>2</sub> ( $C_{\mu}$ ) and the recombination resistance between TiO<sub>2</sub> and the polysulfide electrolyte ( $R_{rec}$ ). Figure 6 illustrates the  $C_{\mu}$  and  $R_{rec}$  of the analyzed samples obtained from IS fitting.<sup>13</sup> Impedance characterization allows separation of the different aspects of the solar cell enabling the study of the sensitized electrode independently of other factors such as series resistance and counter electrode. IS enables extracting the voltage drop in the sensitized electrode,  $V_F$ , at each applied potential,  $V_{appl}$ , by subtracting the effect of the series resistance and counter electrode on both  $R_{rec}$  and  $C_{\mu}$ <sup>32</sup> as follows:  $V_F = V_{appl} - V_s - V_{counter}$ , where  $V_s$  and  $V_{counter}$  are the potential drop at the series resistance and at the counter electrode, respectively.  $V_F$  is proportional to the rise of the Fermi level of electrons in TiO<sub>2</sub>,  $V_F = (E_{Fn} - E_{F0})/q$ , where  $q$  is the positive elementary charge and  $E_{Fn}$  and  $E_{F0}$  are the electron Fermi level and the electron Fermi level at the equilibrium respectively. Figure 6a represents  $C_{\mu}$  as a function of the voltage drop in the sensitized electrode,  $V_F$ . Since the chemical capacitance records the density of states in the TiO<sub>2</sub>, the shift of  $C_{\mu}$  to lower potential for the surface treated samples indicates a downward displacement of the TiO<sub>2</sub> CB. The origin of the shift with ZnS and/or dipole molecules could be that both treatments are preventing the direct contact of the polysulfide electrolyte (pH ~12) with TiO<sub>2</sub>, which decreases the effective “observed” pH of the TiO<sub>2</sub> surface, consequently reducing the TiO<sub>2</sub> CB position.<sup>33,34</sup>

A key factor in explaining solar cell behavior is the recombination resistance  $R_{rec}$ .<sup>35,36</sup> To analyze the recombination resistance on the basis of a similar number of electrons (i.e.,

- (31) Hodes, G.; Manassen, J.; Cahen, D. *J. Electrochem. Soc.* **1980**, *127*, 544.
- (32) Fabregat-Santiago, F.; Bisquert, J.; Palomares, E.; Otero, L.; Kuang, D. B.; Zakeeruddin, S. M.; Gratzel, M. *J. Phys. Chem. C* **2007**, *111*, 6550.
- (33) Mora-Sero, I.; Bisquert, J. *Nano Lett.* **2003**, *3*, 945.
- (34) Fabregat-Santiago, F.; Mora-Seró, I.; Garcia-Belmonte, G.; Bisquert, J. *J. Phys. Chem. B* **2003**, *107*, 758.
- (35) Bisquert, J.; Fabregat-Santiago, F.; Mora-Seró, I.; Garcia-Belmonte, G.; Giménez, S. *J. Phys. Chem. C* **2009**, *113*, 17278.
- (36) Bisquert, J.; Mora-Seró, I. *J. Phys. Chem. Lett.* **2010**, *1*, 450.

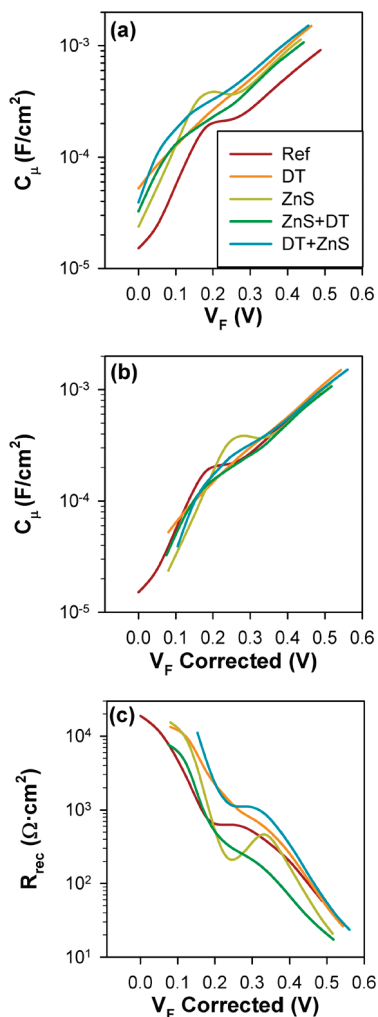


**Figure 6.** Capacitance and recombination resistance obtained from IS for the same samples as that shown in Figure 5. (a) As-measured capacitance. (b) Corrected capacitance by shifting the  $V_F$  to compare samples with the same  $\text{TiO}_2$  conduction band position. (c) Recombination resistance corrected by shifting the same amount as that in (b).

the same distance between Fermi level and CB), the shift of the conduction band (indicated for each sample in Table 1) has been corrected in Figure 6b and 6c, where the voltage scale is  $V_F$  Corrected. The criterion for the modified scale is that the chemical capacitances of all the analyzed samples overlap; see Figure 6b. If the recombination process is identical for all samples, a similar overlap of the recombination resistance should be expected. It is however observed that, at low potentials, the reference sample exhibits lower recombination resistance (i.e., higher recombination) compared to the treated samples (Figure 6c), which explains the higher  $j_{sc}$  measured for the treated samples. On the other hand,  $R_{rec}$  is highly sensitive to the sequence of surface treatments. Samples first treated with the dipole molecules show higher recombination resistance compared to samples first treated with the ZnS coating. The increase in  $R_{rec}$  with the dipoles could be a result of shifting up the CB of the QDs in such a way that the energetic barrier, QDs themselves preventing recombination from  $\text{TiO}_2$  to the electrolyte, becomes larger.

To better understand the solar cell performances shown in Figure 5 and Table 1, these results have to be analyzed considering three interconnected factors: (i) the upward displacement of CdSe CB, as it has been observed from the PV

onset shift (see Figure 2); (ii) the downward displacement of the  $\text{TiO}_2$  CB, observed from  $C_\mu$  shift (Figure 6a); and (iii) the different recombination resistances obtained for the different cells (see Figure 6c). Factors i and ii point to an increase of the photocurrent obtained for the treated samples as a consequence of an increase of the electron injection driving force due to a more favorable QD and  $\text{TiO}_2$  CB alignment. It has been shown that both upward displacement of the QD CB with respect to the  $\text{TiO}_2$  CB<sup>29</sup> and a downward movement of the  $\text{TiO}_2$  CB with respect to the QD CB<sup>37</sup> produce an increase of the electron transfer rate from QD to  $\text{TiO}_2$ . But, this effect is not symmetrical, and a higher increase of the transfer rate is observed with the upward displacement of the QD CB.<sup>29,37</sup> In this sense, even with the clear downward displacement of  $\text{TiO}_2$  CB from IS measurements, the upward movement of the QD CB after dipole treatment cannot be completely ruled out, judging by the dramatic effect on the photocurrent observed after the dipole treatment (see Table 1).

A downward displacement of the  $\text{TiO}_2$  CB is commonly associated with an increase of  $j_{sc}$ , due to a higher electron injection driving force, and a decrease of  $V_{oc}$ , due to a reduction of the splitting between the  $\text{TiO}_2$  Fermi level and redox position.<sup>38</sup> Nevertheless, this implication is not generally the case since recombination plays a determinant role on  $V_{oc}$  as recently pointed out,<sup>39,40</sup> and a reduction of recombination also leads to an increased  $V_{oc}$ . This is the case for the samples first treated with molecular dipoles, DT and DT+ZnS, where the downward displacement of the  $\text{TiO}_2$  CB does not lead to a decrease of  $V_{oc}$ . Indeed, a higher value is observed due to the increase of the recombination resistance. For the ZnS+DT sample, where this strong reduction of recombination is not observed, a reduction of  $V_{oc}$  is detected. These results reflect the extreme importance of  $R_{rec}$  in understanding the solar cell behavior. The nonsymmetric behavior observed between DT+ZnS and ZnS+DT samples likely originates from the direct attaching of molecular dipoles to the QDs. Molecular dipoles can also serve as a hole extraction layer, something that ZnS could not do due to its band position. It has been observed that thiol groups can act as hole traps in CdSe QDs.<sup>41</sup>

Finally it is worth noting the valley observed in Figure 6c for  $R_{rec}$  at potential values between 0.2 and 0.3 V. This behavior has been previously reported,<sup>33,35</sup> and it is ascribed to a recombination between  $\text{TiO}_2$  surface states.<sup>13,33</sup> It is clearly visible for the reference and treated samples with a first treatment with ZnS coating. It correlates with the capacitance plateau region also observed in Figure 6c, due to the band unpinning.<sup>13</sup> This valley is smoothed for samples first treated with molecular dipoles, DT and DT+ZnS, reflecting the effect of the different voltage drops at the intermediate dielectric layer, affecting the broadening of the  $C_\mu$  plateau region and the shape of the  $R_{rec}$  valley.<sup>13</sup>

## Conclusions

A significant increase (600%) of the photovoltaic performance of mesoporous  $\text{TiO}_2/\text{CdSe}$  electrodes could be achieved by

- (37) Chakrapani, V.; Tvrđy, K.; Kamat, P. V. *J. Am. Chem. Soc.* **2010**, *132*, 1228.  
 (38) Fabregat-Santiago, F.; Bisquert, J.; Garcia-Belmonte, G.; Boschloo, G.; Hagfeldt, A. *Sol. Energy Mater. Sol. Cells* **2005**, *87*, 117.  
 (39) Marinado, T.; Nonomura, K.; Nissfolk, J.; Karlsson, M. K.; Hagberg, D. P.; Sun, L.; Mori, S.; Hagfeldt, A. *Langmuir* **2010**, *26*, 2592.  
 (40) Li, R.; Lv, X.; Shi, D.; Zhou, D.; Cheng, Y.; Zhang, G.; Wang, P. *J. Phys. Chem. C* **2009**, *113*, 7469.  
 (41) Wuister, S. F.; de MelloDonega, C.; Meijerink, A. *J. Phys. Chem. B* **2004**, *108*, 17393.

tailoring both charge injection and recombination dynamics by proper surface modification of the nanostructure. The synergistic interaction of the adequate combination of both surface treatments tested in the present study (grafting of molecular dipoles and ZnS coating) is reflected in the increased IPCE and the photovoltaic properties obtained:  $9.74 \text{ mA/cm}^2$  and 1.60% efficiency. In addition, the key role of the surface treatments in recombination control has been stressed to understand the solar cell performance. Finally, it can be concluded that surface treatments allow designing both injection and recombination dynamics for QDSCs. This fact could have important implications for the development of this kind of cells.

**Acknowledgment.** This work was partially supported by the Ministerio de Ciencia e Innovación of Spain under the projects

HOPE CSD2007-00007, JES-NANOSOLAR PLE2009-0042, and MAT2007-62982 and by Generalitat Valenciana under the project ACOMP/2009/095 and PROMETEO/2009/058. The authors acknowledge also the support of the Israeli Science Foundation, Bikura Program. E.M.B. would also like to acknowledge the financial support from the European Science Foundation (ESF) through the activity entitled "New Generation of Organic based Photovoltaic Devices". S.G. acknowledges the Ministerio de Ciencia e Innovación for its support through the Ramón y Cajal program. Dr. Beatriz Julián López is gratefully acknowledged for her support with the diffuse reflectivity measurements.

JA101752D